Research Article | Vol. 27, No. 6 | 18 Mar 2019 | OPTICS EXPRESS 9054
Optics EXPRESS

Single-exposure fabrication of tunable Pancharatnam-Berry devices using a dye-doped liquid crystal

YAN LI,[1,*] YUEDA LIU,[1] SIDA LI,[1] PENGCHENG ZHOU,[1] TAO ZHAN,[2] QUANMING CHEN,[1] YIKAI SU,[1] AND SHIN-TSON WU[2]

[1]*Department of Electronic Engineering, Shanghai Jiao Tong University, Shanghai, 200240, China*
[2]*College of Optics and Photonics, University of Central Florida, Orlando, FL 32816, USA*
**yan.li@sjtu.edu.cn*

Abstract: We report a non-interferometric single-exposure technique for fabricating Pancharatnam-Berry (PB) devices with arbitrary wavefronts, via photo-patterning an azo-dye doped LC with a two-dimensional linear polarization field, whose local polarization direction can be controlled by a spatial light modulator (SLM) on the pixel level. Upon one exposure, different local LC orientations are generated simultaneously. The non-interferometric approach is insensitive to environmental disturbance, and moreover, the dynamic phase mask on the SLM can be conveniently reconfigured by a computer. Our fabricated PB gratings, q-plates and hologram exhibit good optical performances. Such a simple yet reconfigurable fabrication method enables new PB devices to be developed, and it would open a new gateway towards widespread applications.

1. Introduction

Pancharatnam-Berry (PB) phase optical elements [1–5], have attracted great research interest. Instead of generating phase shift based on optical path difference, PB devices generates it by the spatial variation of optical anisotropy. Especially PB devices based on liquid crystals (LCs), exhibit extremely high efficiency in the visible region and offers electro-optic tunability. In addition to deflecting or focusing light in a thin flat form [6–9], PB LC devices are also capable of generating vortex and Bessel beams [10,11], that are extensively used for optical trapping and bio-imaging [12–14]. There are two ways to fabricate PB LC devices. One is using multi-beam interference [15–17] which could possibly record arbitrary physical object's wavefront and generate corresponding PB patterns. But it vulnerable to environmental disturbance and requires coherent light sources. The second approach is by photo-patterning of LCs. PB devices were fabricated by photo patterning through static photo masks [18–20]. However, once fabricated, the static masks cannot be reconfigured, which inevitably increases the fabrication cost and time. Two maskless approaches based on DMD (digital mirror device) based micro-lithography [21–23], and direct laser writing [17,24–26], respectively, were reported, which could realize arbitrary PB devices without a photo mask. However, both techniques can only realize one orientation direction for each exposure. Thus, multiple-step exposure and high-precision mechanical rotation of polarizers are still required. De Sio et. al. proposed a digital polarization holography method for fabricating arbitrarily-patterned phase PB devices, by using two quarter wave plates (QWPs) and a spatial light modulator (SLM), but the polymerized LC PB devices they fabricated lacked electro-optical switchability [27].

Here, we propose a non-interferometric single-exposure approach for fabricating switchable PB LC devices with arbitrary wavefronts. By appropriately arranging a polarizer, a spatial light modulator and a quarter wave plate, a high resolution two-dimensional (2D) linear polarization field was generated, and then used to photo-pattern an azo-dye-doped LC

#358299 https://doi.org/10.1364/OE.27.009063
Journal © 2019 Received 21 Jan 2019; revised 26 Feb 2019; accepted 3 Mar 2019; published 13 Mar 2019

Optics EXPRESS

mixture. After a one-step photo-patterning, different local orientations can be realized simultaneously, forming PB devices with arbitrary phase distributions. To prove the concept, in this paper we have fabricated several PB devices, including PB gratings, q-plates, and a PB hologram. This simple fabrication technique features low cost, single-step exposure, high resolution, reconfigurable phase mask and quasi-continuous pattern variation. In addition, this non-interferometric approach is insensitive to environmental disturbance, and free of any mechanical movement. Thus, it could significantly facilitate the fabrication of PB devices for widespread applications.

2. Result

Theory: from phase retardation to polarization rotation

The basic principle of realizing polarization rotation by controlling phase retardation in our proposed approach is schematically illustrated in Fig. 1(a). The incident light passes through a polarizer, a uniaxial phase retarder and a QWP successively. Here, the light propagation direction is along z axis, and the transmission axis of the polarizer is in y direction. The slow axes of the retarder and the QWP are at 45 ^{o} and 0 ^{o} with respect to the y direction, respectively in the x-y plane. Based on Jones Matrix, the output electric vector can be derived as:

$$E_{out}=\begin{bmatrix} e^{-\frac{\pi}{4}j} & 0 \\ 0 & e^{\frac{\pi}{4}j} \end{bmatrix}\begin{bmatrix} \cos 45^o & \sin 45^o \\ -\sin 45^o & \cos 45^o \end{bmatrix}\begin{bmatrix} e^{-j\frac{\delta}{2}} & 0 \\ 0 & e^{j\frac{\delta}{2}} \end{bmatrix}\begin{bmatrix} \cos 45^o & -\sin 45^o \\ \sin 45^o & \cos 45^o \end{bmatrix}\begin{bmatrix} 0 & 0 \\ 0 & 1 \end{bmatrix}\begin{bmatrix} E_{xin} \\ E_{yin} \end{bmatrix}=je^{-\frac{\pi}{4}j}E_{yin}\begin{bmatrix} \sin\frac{\delta}{2} \\ \cos\frac{\delta}{2} \end{bmatrix} \quad (1)$$

where E_{xin} and E_{yin} are the x and y components of the input electric field, respectively; and δ is the phase retardation of the uniaxial retarder. From Eq. (1), the output electric field is linearly polarized with its polarization direction oriented at δ/2 to the y axis. Thus, using such a simple configuration, the polarization rotation angle can be precisely controlled by the phase retardation. The nature of generating such a linear polarization with controllable direction could be also understood in the following way. The linearly polarized o-ray and e-ray in the uniaxial retarder have equal amplitude but a δ phase difference. After passing through the QWP, they become circular polarizations (with opposite handedness and δ phase difference) and got superposed, generating a linear polarization whose direction is determined by δ. Since such superposition is carried out in a single-beam non-interferometric configuration, it is much less sensitive to environmental disturbance than the two-beam interference approaches.

To verify this concept, we carried out a proof-of-concept experiment using a 6-μm homogeneous-alignment cell filled with a nematic liquid crystal (E7, HCCH), as the uniaxial retarder in Fig. 1(a). When a voltage is applied between the two planar Indium tin oxide (ITO) electrodes of the cell, an electric field is induced perpendicular to the substrates, inducing LC molecules to rotate and phase retardation to decrease. First, the phase retardation δ of the cell at different voltage was obtained by measuring the transmittance under crossed polarizers [28]. After that, the LC cell was inserted in the configuration shown in Fig. 1(a), as the uniaxial retarder. The output linear polarization was then examined by an additional polarizer (not shown in Fig. 1(a)) behind the QWP, as the applied voltage on the LC cell varied. Such a polarizer, for analyzing the polarization characteristic, will be referred to as an analyzer. From the data in Fig. 1(b), one can see that indeed polarization rotation angle ϕ is approximately a half of phase retardation, δ/2, as predicted by Eq. (1).

Optics EXPRESS

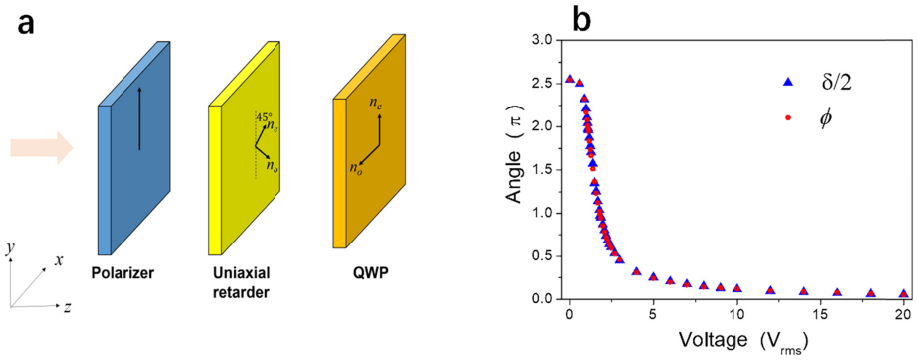

Fig. 1. (a) Schematic illustration of apparatus used to tune polarization rotation angle ϕ by phase retardation δ. (b) Half of phase retardation δ/2 and polarization rotation angle ϕ at different applied voltage for a nematic E7 LC cell with a cell gap of 6 μm at 532 nm.

If the uniaxial retarder in Fig. 1(a) is replaced by a SLM, whose phase retardation could be precisely controlled on the pixel level, then an arbitrary 2D polarization direction distribution could be generated, enabling the fabrication of PB devices with arbitrary patterns. Figure 2(a) depicts our proposed fabrication system. The system consists of a laser, a beam expander (lenses L1 and L2), a polarizer, a reflective liquid-crystal-on-Silicon SLM, a QWP and an imaging lens L3. The optic axes of the polarizer, SLM and QWP are oriented in the same way as in Fig. 1(a). The SLM used in the experiment is a pure phase SLM (model: PLUTO-VIS, Holoeye) with homogeneous alignment. The function of lens L3 is to image the SLM onto the sample position. The generated light pattern is then used to align LC molecules and form PB devices. Specifically, in our experiment, the LC cells were filled a mixture consisting of 99% E7 and 1% photo-sensitive azo-dye methyl red (MR, Sigma Aldrich). Upon illumination, MR molecules undergo trans-cis transformation, inducing diffusion and adsorption onto the substrates [19]. After many trans-cis cycles, the MR molecules reach a stable state when their long axes are approximately perpendicular to the pumping-beam polarization. Meanwhile, the absorbed dye aligns the LC accordingly, forming spatial-varying anisotropy that is determined by pre-designed grey-level pictures loaded on the SLM. The green laser used in the experiment has a center wavelength at 532 nm where MR has a reasonably high absorption.

Before the fabrication could be implemented, the polarization-rotation property of the system needs to be characterized. An analyzer (not shown in the figure) was inserted between L3 and the image plane, to examine the output polarization. When the SLM was loaded with uniform grey-level pictures, the analyzer was rotated to obtain minimum light intensity, so that its absorption axis was parallel to the output linear polarization. The measured orientation angle of the analyzer versus grey level is plotted in Fig. 2(b). Since the SLM could provide more than 3π phase change for 532 nm, the polarization rotation range is more than 300° as grey level goes from 0 to 255, as Fig. 2(b) shows. Such a wide range is more than enough for realizing arbitrary LC orientation. Moreover, a very fine angular resolution (1°) could be achieved, implying feasible realization of quasi-continuous orientation variation.

Optics EXPRESS

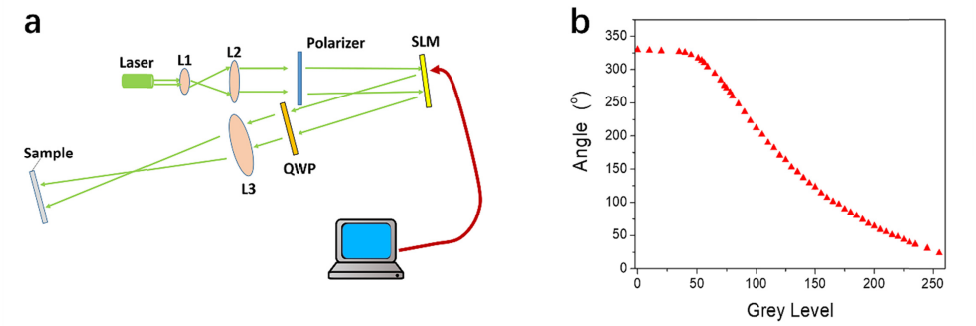

Fig. 2. (a) Optical setup of the proposed fabrication technique. (b) Analyzer angle versus grey-levels when minimum light intensity is achieved.

Utilizing the data in Fig. 2(b), we first generated a polarization pattern with three orientation domains (star, rectangle, and background as shown in Fig. 3) by marking them with different grey levels. Figure 3(a) is a photo of the light pattern taken by a camera through a polarizer. One can see that the three domains appear with different brightness, because each possesses a different polarization direction. Then a cell (Cell 1, 3 μm, no alignment layer) filled with the MR-LC mixture was placed in the image plane of the SLM, as shown in Fig. 2, and exposed by the polarization pattern with light intensity ~40 mW/cm^2 for 10 minutes. The temperature of the LC cell was kept at 67°C (isotropic) during the whole exposure process to realize double-side photo alignment [19].

After exposure, three domains with different MR/LC orientations were generated simultaneously. Figure 3(b) is a picture of Cell 1 when it was illuminated by a linearly-polarized white light. Due to the anisotropic absorption of MR in the visible region, the three domains, with different MR orientations, exhibit different light intensity. Figure 3(c) shows the picture of Cell 1 when it was sandwiched between crossed polarizers with red light illumination. Since MR has negligible absorption in red, the transmittance variation in different domains is attributed to different LC orientations. We also fabricated Cell 2 (3 μm, no alignment layer) with an elliptical pattern, where both MR and LC orientations varied linearly from 0° to 90°, from the center to the edge. Figure 3(d) shows the photos taken when the cell was rotated under linearly-polarized white illumination. One can see that quasi-continuous pattern variation is realized in the MR/LC material.

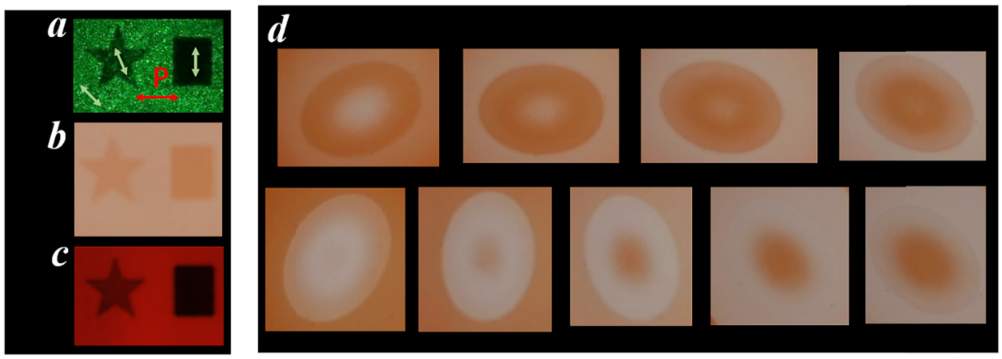

Fig. 3. (a) Light pattern with different local polarization orientations, captured through a polarizer. The red arrow indicates transmission axis direction of the polarizer. Light-green arrows indicate linear polarization directions in different domains. (b) Photo of Cell 1, illuminated by a linearly-polarized white light. (c) Photo of Cell 1, under crossed polarizers, illuminated by red light. (d) Photos of Cell 2 rotated at different orientations, under linearly-polarized white illumination.

Optics EXPRESS

To demonstrate the versatility of this fabrication method, we prepared several functional PB devices, including gratings, q-plates and a hologram, using the same LC mixture and the same type of cells. Figures 4(c) and 4(f) show the microscopic pictures of a binary grating and a continuous grating, respectively. The LC directors are perpendicular to each other in adjacent regions in the binary grating, while those in the continuous grating vary from 0° to 180° with an increment of 30°. Both gratings have a period of 48 μm. Figures 4(a) and 4(b) show the diffraction patterns of the binary grating when the voltage was turned off and on, respectively. And Figs. 4(d) and 4(e) show the diffraction patterns for the continuous polarization grating. The electro-optic property of the continuous grating was investigated using a circularly-polarized probing beam generated from a He-Ne laser (632.8 nm). The intensity of the first order at different applied voltage was measured. The normalized diffraction efficiency versus voltage curve for the first order is plotted in Fig. 4(g). Dots are measured data and the solid line represents simulated result. The diffraction efficiency of a PB device at the voltage-off state is $\eta = \sin^2(\pi\Delta n d/\lambda)$ [29], where d is the cell gap, λ is the wavelength and Δn is the birefringence of the liquid crystal. Here, the thickness of the cell is approximately 3 μm and Δn of E7 is about 0.225, so for 632.8 nm, $\pi\Delta n d/\lambda \sim \pi$, resulting in nearly zero diffraction efficiency. As voltage is applied between the two planar ITO electrodes of the cell, LC directors tend to rotate to be parallel to the electric field (perpendicular to the substrates). Hence, the effective refractive index difference between the *o* wave and *e* wave decreases, and the phase retardation gets smaller with increased voltage. A peak diffraction efficiency ~95.3% is obtained at ~1.6 V_{rms} when the phase retardation satisfies the half-wave retardation condition [30,31]. The measured rise time and decay time of the continuous PB grating is 100 ms and 10 ms, respectively. The slow rise time originates from the fact that the peak-efficiency voltage (1.6 V_{rms}) is relatively close to the threshold (~1 V). To speed up the rise time, overdrive voltage method has been commonly practiced [32].

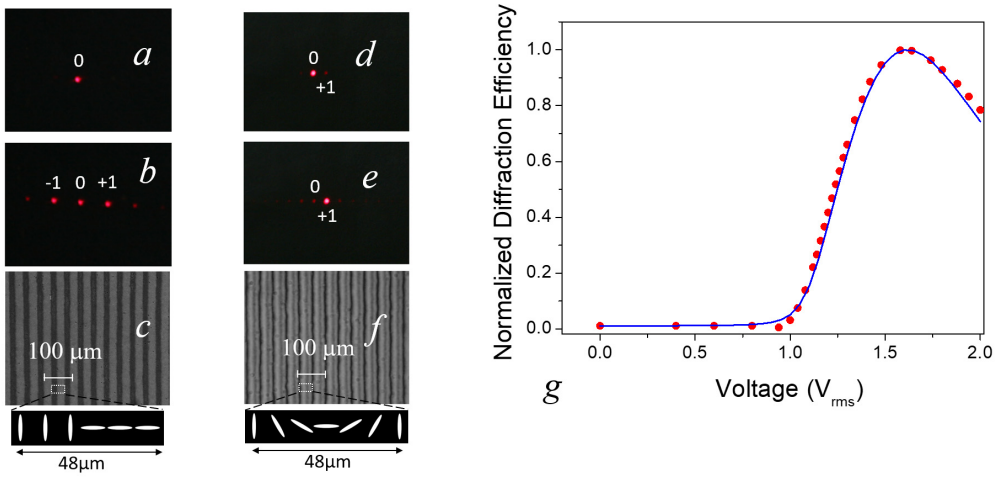

Fig. 4. Diffraction patterns of a binary PB grating at (a) voltage-off and (b) voltage-on states. (c) Microscopic morphology of the binary PB grating. Diffraction patterns of the continuous PB grating at d) voltage-off and (e) voltage-on states. (f) Microscopic morphology of a continuous PB grating. (g) Voltage dependent first-order diffraction efficiency of the continuous PB grating: dots are measured data and solid line is simulation result.

We fabricated four q-plates [17,31,33] with topological charge m = 0.5, 1, 1.5 and 2. The microscopic pictures of the q-plates under crossed polarizers are shown in Figs. 6(a)-6(d). One can see that the LC alignment variation is quite smooth. The vortex light patterns generated using circularly polarized illumination from the He-Ne laser were captured by a CCD camera and results are shown in Figs. 5(e)-5(h). As m increases, the radius of the final optical field is enlarged gradually.

Optics EXPRESS

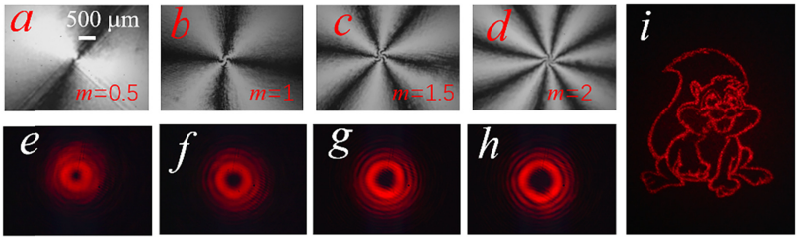

Fig. 5. Microscopic morphologies of the PB q-plates: (a) m = 0.5, (b) m = 1, (c) m = 1.5, and (d) m = 2. Far field light pattern captured by a CCD camera: (e) m = 0.5, (f) m = 1, (g) m = 1.5 and (h) m = 2. (i) Reconstructed image from a PB hologram.

We also fabricated a PB hologram [34] using the dye-doped LC. Holograms are important optical elements which contain the complete information of an object wave. Traditional phase-type holograms are fabricated using photorefractive materials, photopolymer films and so on, and their phase modulation is usually realized by refractive index variation. As for PB holograms, the phase modulation is accomplished by LC director variation. The phase pattern was first obtained based on Gerchberg-Saxton iteration algorithm [35]. And then the phase distribution was mapped to LC orientation variation according to $\phi = \delta/2$, and finally to a grey-level picture based on the data plotted in Fig. 2(b). As the fabricated PB hologram was illuminated by a red He-Ne laser beam, a holographic image with high definition was reconstructed as shown in Fig. 5(i).

3. Conclusion and discussion

We have developed a non-interferometric single-exposure technique for fabricating PB devices with arbitrary anisotropy pattern. A 2D polarization pattern, with a spatial resolution of 1920 x 1080, and angular resolution ~1°, is generated to photo-pattern a dye-doped LC mixture for realizing different local anisotropy orientations simultaneously. The resolution of this photo alignment technique is mainly determined by the imaging system and the SLM resolution. In our experiment, we used an imaging system with a magnification factor of "1", and a SLM with a pixel size of 8 μm. So theoretically, the smallest domain we can control its polarization on the sample is the same as the SLM pixel size, 8 μm. By using an imaging system with a smaller magnification factor, higher resolution could be achieved. The polarization pattern could be dynamically updated by the computer-controlled SLM, without the need for pre-designed masks. The non-interferometric nature of the configuration, makes it more tolerable to environmental disturbance. The single-step exposure, greatly simplifies the fabrication process and increases yield. Hence, such a simple fabrication technique has great potential for various PB device fabrications.

Funding

The National Natural Science Foundation of China (61727808) and Shanghai Jiao Tong University (YG2016QN37).

References

1. J. Anandan, "The geometric phase," Nature **360**(6402), 307–313 (1992).
2. S. Pancharatnam, "Generalized theory of interference, and its applications," Proc. Ind. Acad. Sci. A **44**(6), 398–417 (1956).
3. M. V. Berry, "Quantum phase factors accompanying adiabatic changes," Proc. R. Soc. Lond. A Math. Phys. Sci. **392** (1802), 45–57 (1984).
4. G. Zheng, H. Mühlenbernd, M. Kenney, G. Li, T. Zentgraf, and S. Zhang, "Metasurface holograms reaching 80% efficiency," Nat. Nanotechnol. **10**(4), 308–312 (2015).
5. U. Levy, C. H. Tsai, H. C. Kim, and Y. Fainman, "Design, fabrication and characterization of subwavelength computer-generated holograms for spot array generation," Opt. Express **12**(22), 5345–5355 (2004).

Optics EXPRESS

6. C. Oh and M. J. Escuti, "Achromatic diffraction from polarization gratings with high efficiency," Opt. Lett. **33**(20), 2287–2289 (2008).
7. R. K. Komanduri and M. J. Escuti, "High efficiency reflective liquid crystal polarization gratings," Appl. Phys. Lett. **95**(9), 091106 (2009).
8. J. Kim, C. Oh, S. Serati, and M. J. Escuti, "Wide-angle, nonmechanical beam steering with high throughput utilizing polarization gratings," Appl. Opt. **50**(17), 2636–2639 (2011).
9. T. Zhan, Y.-H. Lee, and S.-T. Wu, "High-resolution additive light field near-eye display by switchable Pancharatnam-Berry phase lenses," Opt. Express **26**(4), 4863–4872 (2018).
10. B. Y. Wei, W. Hu, Y. Ming, F. Xu, S. Rubin, J. G. Wang, V. Chigrinov, and Y. Q. Lu, "Generating switchable and reconfigurable optical vortices via photopatterning of liquid crystals," Adv. Mater. **26**(10), 1590–1595 (2014).
11. B. Wei, S. Liu, P. Chen, S. Qi, Y. Zhang, W. Hu, Y. Lu, and J. Zhao, "Vortex Airy beams directly generated via liquid crystal q-Airy-plates," Appl. Phys. Lett. **112**(12), 121101 (2018).
12. M. Woerdemann, C. Alpmann, M. Esseling, and C. Denz, "Advanced optical trapping by complex beam shaping," Laser Photonics Rev. **7**(6), 839–854 (2013).
13. S. W. Hell and J. Wichmann, "Breaking the diffraction resolution limit by stimulated emission: stimulated-emission-depletion fluorescence microscopy," Opt. Lett. **19**(11), 780–782 (1994).
14. J. Fölling, M. Bossi, H. Bock, R. Medda, C. A. Wurm, B. Hein, S. Jakobs, C. Eggeling, and S. W. Hell, "Fluorescence nanoscopy by ground-state depletion and single-molecule return," Nat. Methods **5**(11), 943–945 (2008).
15. V. Presnyakov, K. Asatryan, T. Galstian, and V. Chigrinov, "Optical polarization grating induced liquid crystal micro-structure using azo-dye command layer," Opt. Express **14**(22), 10558–10564 (2006).
16. Y. Li, J. Kim, and M. J. Escuti, "Orbital angular momentum generation and mode transformation with high efficiency using forked polarization gratings," Appl. Opt. **51**(34), 8236–8245 (2012).
17. J. Kim, Y. Li, M. N. Miskiewicz, C. Oh, M. W. Kudenov, and M. J. Escuti, "Fabrication of ideal geometric-phase holograms with arbitrary wavefronts," Optica **2**(11), 958–964 (2015).
18. W. Hu, A. Kumar Srivastava, X.-W. Lin, X. Liang, Z.-J. Wu, J.-T. Sun, G. Zhu, V. Chigrinov, and Y.-Q. Lu, "Polarization independent liquid crystal gratings based on orthogonal photoalignments," Appl. Phys. Lett. **100**(11), 111116 (2012).
19. L. C. Lin, H. C. Jau, T. H. Lin, and A. Y. Fuh, "Highly efficient and polarization-independent Fresnel lens based on dye-doped liquid crystal," Opt. Express **15**(6), 2900–2906 (2007).
20. Y. Guo, M. Jiang, C. Peng, K. Sun, O. Yaroshchuk, O. Lavrentovich, and Q.-H. Wei, "High-resolution and high-throughput plasmonic photopatterning of complex molecular orientations in liquid crystals," Adv. Mater. **28**(12), 2353–2358 (2016).
21. C. Culbreath, N. Glazar, and H. Yokoyama, "Note: Automated maskless micro-multidomain photoalignment," Rev. Sci. Instrum. **82**(12), 126107 (2011).
22. H. Wu, W. Hu, H. C. Hu, X. W. Lin, G. Zhu, J. W. Choi, V. Chigrinov, and Y. Q. Lu, "Arbitrary photo-patterning in liquid crystal alignments using DMD based lithography system," Opt. Express **20**(15), 16684–16689 (2012).
23. C. Sun, N. Fang, D. M. Wu, and X. Zhang, "Projection micro-stereolithography using digital micro-mirror dynamic mask," Sens. Actuators A Phys. **121**(1), 113–120 (2005).
24. M. E. McConney, A. Martinez, V. P. Tondiglia, K. M. Lee, D. Langley, I. I. Smalyukh, and T. J. White, "Topography from topology: photoinduced surface features generated in liquid crystal polymer networks," Adv. Mater. **25**(41), 5880–5885 (2013).
25. M. N. Miskiewicz and M. J. Escuti, "Direct-writing of complex liquid crystal patterns," Opt. Express **22**(10), 12691–12706 (2014).
26. M. N. Miskiewicz and M. J. Escuti, "Optimization of direct-write polarization gratings," Opt. Eng. **54**(2), 025101 (2015).
27. L. De Sio, D. E. Roberts, Z. Liao, S. Nersisyan, O. Uskova, L. Wickboldt, N. Tabiryan, D. M. Steeves, and B. R. Kimball, "Digital polarization holography advancing geometrical phase optics," Opt. Express **24**(16), 18297–18306 (2016).
28. D. K. Yang and S. T. Wu, *Fundamentals of Liquid Crystal Devices* (Wiley, 2006), page 76.
29. Y. H. Lee, G. Tan, T. Zhan, Y. Weng, G. Liu, F. Gou, F. Peng, N. V. Tabiryan, S. Gauza, and S. T. Wu, "Recent progress in Pancharatnam-Berry phase optical elements and the applications for virtual/augmented realities," Opt. Data Process. Storage **3**(1), 79–88 (2017).
30. L. Nikolova and P. S. Ramanujam, *Polarization Holography* (Cambridge University, 2009).
31. L. Marrucci, C. Manzo, and D. Paparo, "Pancharatnam-Berry phase optical elements for wavefront shaping in the visible domain: switchable helical modes generation," Appl. Phys. Lett. **88**(22), 221102 (2006).
32. S. T. Wu, "Nematic liquid crystal modulator with response time less than 100 μs at room temperature," Appl. Phys. Lett. **57**(10), 986–988 (1990).
33. W. Ji, C. H. Lee, P. Chen, W. Hu, Y. Ming, L. Zhang, T. H. Lin, V. Chigrinov, and Y. Q. Lu, "Meta-q-plate for complex beam shaping," Sci. Rep. **6**(1), 25528 (2016).
34. X. Xiang, M. N. Miskiewicz, and M. J. Escuti, "Distortion-free broadband holograms: a novel class of elements utilizing the wavelength independent geometric phase," Proc. SPIE **9386**, 938609 (2015).
35. 35. R. W. Gerchberg and W. O. Saxton, "A practical algorithm for the determination of phase from image and diffraction plane pictures," Optik (Stuttg.) 35(2), 227–246 (1972).